Geometry and dynamics in the Fresnel transforms of discrete systems

Kurt Bernardo Wolf* and Guillermo Krötzsch

Instituto de Ciencias Físicas, Universidad Nacional Autónoma de México, Cuernavaca, Morelos 62251, México
**Corresponding author: bwolf@fis.unam.mx*

Received March 6, 2007; revised April 11, 2007; accepted April 16, 2007;
posted April 20, 2007 (Doc. ID 80565); published July 19, 2007

Free propagation in continuous optical and mechanical systems is generated by the momentum-squared operator and results in a shear of the phase space plane along the position coordinate. We examine three discrete versions of the Fresnel transform in periodic systems through their Wigner function on a toroidal phase space. But since it is topologically impossible to continuously and globally shear a torus, we examine a fourth version of the Fresnel transform on a spherical phase space, in a model based on the Lie algebra of angular momentum, where the corresponding Fresnel transform wrings the sphere. © 2007 Optical Society of America

OCIS codes: 070.2590, 070.6020, 070.6760, 090.1970.

1. INTRODUCTION

The Fresnel transform describes the evolution of free systems. It is an approximation to the diffraction of traveling waves in Fourier optics [1,2], and also represents the free time evolution of quantum wave functions [3] in homogeneous space. The set of Fresnel transforms $\mathcal{F}(z)$, $z \in \mathsf{R}$, is a one-parameter Lie group generated by the second-derivative operator or, in quantum mechanics, the square momentum operator ([4], [Part IV]). It produces a *shear* of the phase space plane, $\mathcal{F}(z):(x,p)\mapsto(x+zp,p)$ [5]. In this paper we examine various *finite* versions of the Fresnel transform in discrete models of free systems, where the position and momentum coordinates take values on a finite collection of points $\{x_m\}_{m=1}^N$, either periodic modulo N, or nonperiodic.

The first finite version of the Fresnel transform operator, which we indicate by $\mathcal{F}^{[1]}(z)$, is the exponential of the second-difference $N\times N$ matrix. The second version, $\mathcal{F}^{[2]}(z)$, is built as the Fourier transform of a Fresnel lens that impresses a Gaussian phase on the N data points of an input signal. The third, $\mathcal{F}^{[3]}$, follows the discrete Fresnel transform studied by Arrizón and Ojeda-Castañeda [6–8], also used as a model for precession tomography by Leonhardt [9]; this is represented by a discrete Gaussian matrix kernel. We compare these three versions of finite Fresnel transforms through their action on a discrete (periodic) rectangle function, examining their Wigner functions on a discrete phase space torus. Finally, a fourth finite version, $\mathcal{F}^{[\mathrm{K}]}(z)$, which we call Fresnel–Kravchuk transform will be constructed using the su(2) finite oscillator model developed in Cuernavaca [10,11], and its corresponding Wigner function on a sphere [12,13]. Because Fresnel evolution is generated by an su(2) operator squared, we have a global shear—an aberration—of phase space.

It is to be expected that there can be many finite versions of an integral transform, because finite systems generally have a richer structure than continuous ones. This was the case of their fractional Fourier transforms investigated in [14]. The basic condition that all finite versions of a continuous transform must fulfill is that when the interval and density of the data points increase to infinity, the former should contract to the latter. The choice among the various versions of a transform can be influenced by criteria of consistency with geometric and dynamic properties of Hamiltonian systems, such as canonicity and/or/versus unitarity, as well as their computational convenience.

In Section 2 we review the continuous Fresnel transform and Wigner function, whose discrete counterparts are our main interest. We consider periodic N-point signals as represented by their Wigner function on the discrete toroidal phase space and their symmetries in Section 3. In these terms, in Sections 4–6 we plot the three versions of the finite Fresnel transform on a periodic signal and on phase space. In particular, we point out the fourfold quasi-repetition of the Wigner function pattern and the result of the topological obstruction due to the hole of the torus. Thus in Section 7 we propose a version of the finite Fresnel transform on N-point signals that is nonperiodic. The corresponding phase space can be projected on a sphere [12,13]; its corresponding Wigner function is reviewed in Section 8, giving results for the same input signal of the previous sections. The concluding Section 9 compares the two phase space arenas and offers some further comments on the treatment of aberrations of finite signals.

2. FRESNEL TRANSFORMS AND WIGNER FUNCTIONS

We first organize some basic facts of the continuous Fresnel transform [1] and the Wigner function. Paraxial free flight in geometric optics and in classical mechanics is a linear and canonical transformation of phase space $(x,p)\in\mathsf{R}^2$ (where $x\in\mathsf{R}$ is the coordinate of position and $p\in\mathsf{R}$ is momentum, or paraxial ray inclination in geomet-

ric optics). The Fresnel transform $\mathcal{F}(z):(x,p)\mapsto(x(z),p(z))$ shears phase space by a "distance" parameter $z\in\mathsf{R}$ as

$$\begin{pmatrix}x(z)\\p(z)\end{pmatrix}=\begin{pmatrix}1 & z\\0 & 1\end{pmatrix}\begin{pmatrix}x(0)\\p(0)\end{pmatrix}. \tag{1}$$

This is shown in Fig. 1. Under linear transformations, classical and wave models follow each other [2,3], and are canonical ([15], [Part III]). For one-dimensional systems, phase space is a plane; there, canonicity is equivalent to the conservation of area, and no coordinate discontinuities should occur. We expect that appropriate finite models will follow suit.

In wave models, the Schrödinger operators of position $\mathcal{X}:f(x)=xf(x)$ and momentum $\mathcal{P}:f(x)=-\mathrm{i}\mathrm{d}f(x)/\mathrm{d}x$, satisfy the well-known Heisenberg commutation relation $[\mathcal{X},\mathcal{P}]=\mathrm{i}1$. The purely kinetic, free-propagation Hamiltonian is $\frac{1}{2}\mathcal{P}^2$; its Lie exponential is the Fresnel operator $\mathcal{F}(z)$, defined on the space of infinitely differentiable functions of fast decrease on the real line, which is dense in the Hilbert space of all square-integrable functions. There, this operator is represented by the Fresnel integral transform,

$$\mathcal{F}(z):=\exp\left(-\mathrm{i}\tfrac{1}{2}z\mathcal{P}^2\right), \tag{2}$$

$$\mathcal{F}(z)\begin{pmatrix}\mathcal{X}\\\mathcal{P}\end{pmatrix}\mathcal{F}(-z)=\begin{pmatrix}1 & z\\0 & 1\end{pmatrix}\begin{pmatrix}\mathcal{X}\\\mathcal{P}\end{pmatrix}=\begin{pmatrix}\mathcal{X}+z\mathcal{P}\\\mathcal{P}\end{pmatrix}. \tag{3}$$

$$(\mathcal{F}(z):f)(x)=\frac{1}{\sqrt{2\pi\mathrm{i}z}}\int_{\mathsf{R}}\mathrm{d}x'\exp\left(\frac{\mathrm{i}}{2z}(x-x')^2\right)f(x'). \tag{4}$$

The transforms are unitary and form a continuous one-parameter group: $\mathcal{F}(z_1)\mathcal{F}(z_2)=\mathcal{F}(z_1+z_2)$ and $\mathcal{F}(0)=1$. [When the parameter z is analytically continued to the lower complex half-plane, $\mathrm{Im}\,z<0$, the Fresnel transform becomes the Gauss–Weierstrass, or heat diffusion transform ([4], Chap. 9)].

As in quantum mechanics [16,17], signals on a one-dimensional "input" screen, $f(x)$, can be analyzed through their Wigner function on paraxial optical phase space $(x,p)\in\mathsf{R}^2$ [18],

$$W(f|x,p):=\frac{1}{2\pi}\int_{\mathsf{R}}\mathrm{d}y f(x-y)^*\exp(2\mathrm{i}yp)f(x+y). \tag{5}$$

In Fig. 2 we show a rectangle test function ($\mathrm{Rect}_{x_1,x_2}(x)$, equal to 1 in $[x_1,x_2]$ and 0 outside) and the corresponding Wigner function on a portion of phase space; this shears classically under Fresnel transforms (1) [5], as in Fig. 1, namely,

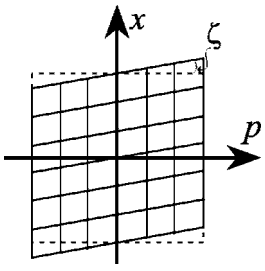

Fig. 1. Fresnel transform $\mathcal{F}(z)$ shears classical phase space $(x,p)\in\mathsf{R}^2$ by the angle $\zeta:=\arctan z$.

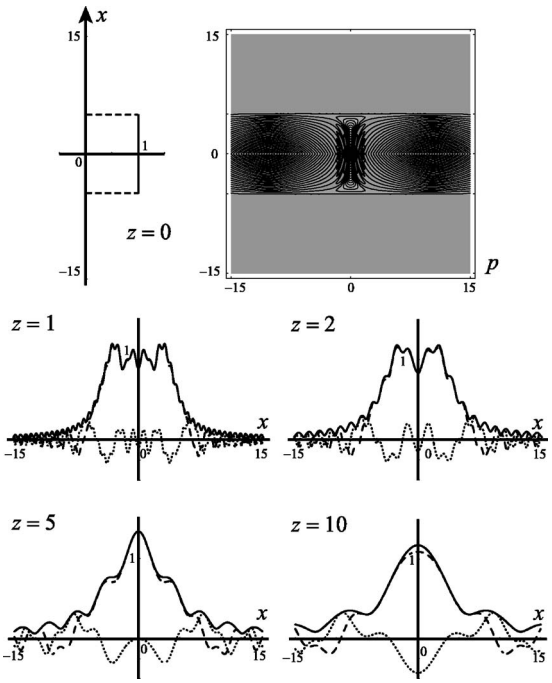

Fig. 2. Top, rectangle signal $f(x)=\mathrm{Rect}_{-5,5}(x)$ and its Wigner function on phase space $W(f|x,p)$ for $x,p\in[-15,15]$ and 20 contours. The x axes are drawn vertically, as if the function represented a light signal on an input screen. Bottom, Fresnel transforms of the rectangle function for $z=1,2,5,10$; real, imaginary, and absolute values are indicated by dashed, dotted, and continuous curves, respectively. These will be compared with their discrete Fresnel versions below.

$$W(\mathcal{F}(z):f|x,p)=W(f|x+zp,p). \tag{6}$$

Also in Fig. 2 are the (continuous) Fresnel transforms of a rectangle function for various values of z; these will be compared with various finite versions of the Fresnel transform below.

Finite and periodic analogs for N-point signals $\mathbf{f}=\{f_m\}$ can be obtained when $f(x)$ is chosen to be a periodic Dirac comb function with coefficients $f_m=f_{m\pm N}$ and "discretizing" the coordinates by

$$x\leftrightarrow 2\pi m/N,\quad \text{for } m \text{ integer modulo } N. \tag{7}$$

When N is odd, convenience dictates the symmetric range of integers $m\in\left[-\frac{1}{2}(N-1),\frac{1}{2}(N-1)\right]$. From this N-vector space of signals, whose values are the coordinates along axes designated by the N positions, the finite Fourier transform yields a canonically conjugate momentum (discrete wavenumber) equivalent N-vector space, along axes designated by $p\leftrightarrow k$, with integer k also counted modulo N. When N is even, quoting Leonhardt [9], "it is probably in the nature of things that discrete Wigner functions for even-dimensional systems are a bit odd,…"; we shall thus consider only N odd. The discrete analog Wigner function defined in Eq. (50) in [9] (see also [19]) is

$$W(\mathbf{f}|m,k):=\frac{1}{N}\sum_n f^*_{m-n}\exp\left(\frac{4\pi\mathrm{i}}{N}kn\right)f_{m+n}, \tag{8}$$

where henceforth we write Σ_n for $\Sigma_{n=-(N-1)/2}^{(N-1)/2}$. This phase space is the discrete torus of integer points (m,k) modulo N, as shown in Fig. 3.

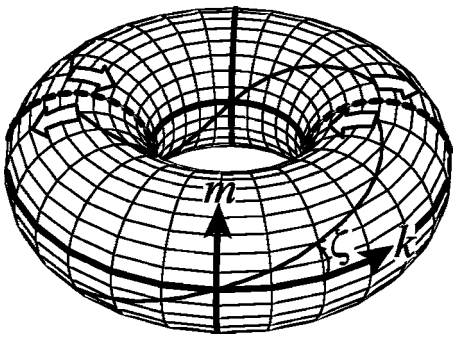

Fig. 3. Discrete toroidal phase space of integer positions m and momenta k counted modulo N. (The two circles are supposed to have the same radius; for visibility they are drawn unequal.) The finite Fresnel transformations $\mathcal{F}^{[z]}(z)$ classically shear the (continuous) torus by angles $\zeta := \arctan z$. The torus breaks at the two circles $k \approx \pm \frac{1}{4}N$.

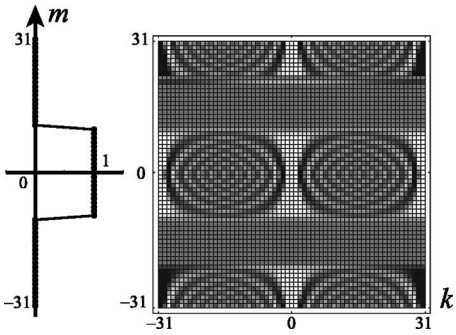

Fig. 4. Left, discrete (and periodic) centered rectangle function $\mathrm{Rect}_{-10,10}(m)$ for $N=63$. For visibility, the data points are joined by continuous lines. Right, the corresponding Wigner function on the discrete toroidal phase space (k,m), shown as pixellated; the upper and lower boundaries of the square represent the same line, as do the right and left boundaries. The center $(0,0)$ corresponds to the "front end" of the torus in Fig. 3.

The Wigner function (8) of a finite, periodic rectangle signal on this toroidal phase space is displayed by the pixellated square in Fig. 4. There is ample literature on discrete, periodic time–frequency distributions (for example, see [20]).

In continuous systems, the only phase space distribution function that is covariant under all linear canonical transformations and (noncommuting) translations, is the original Wigner function (5) [5,16], which is built with the Weyl ordering (sum of all permutations of the individual symbols $\mathcal{X}$, $\mathcal{P}$, divided by the factorial of their number) of all monomials in $\exp \mathrm{i}(x\mathcal{X}+p\mathcal{P})$. The discrete analog (8) is also built with the Weyl ordering of the corresponding finite matrices (see [21], Chap. 2); it is covariant under integer translations but not under linear transformations that map the integer points on the torus out of integer values.

3. WIGNER FUNCTION ON THE TORUS

Since we are working with the example of a centered rectangle signal, we should state the covariance and symmetry properties of the periodic Wigner function (8), which is real. It is covariant of course under integer displacements:

$$g_m = f_{m+m_o} \Rightarrow W(g|m,k) = W(f|m+m_o,k), \tag{9}$$

$$h_m = e^{2\pi \mathrm{i} k_o m/N} f_m \Rightarrow W(h|m,k) = W(f|m,k+k_o). \tag{10}$$

Signals of definite parity have Wigner functions that are invariant under inversions, while signals that are either real or pure imaginary have Wigner functions that are even in momentum,

$$f_{-m} = \pm f_m \Rightarrow W(f|m,k) = W(f|-m,-k), \tag{11}$$

$$f^*_m = \pm f_m \Rightarrow W(f|m,k) = W(f|m,-k). \tag{12}$$

Fresnel transforms do not change the parity of the signal, but they do complexify it, so the $k \leftrightarrow -k$ reflection symmetry of the Wigner function (12) is lost under free propagation.

Additionally, we should comment on other symmetries of the Wigner function on the torus that are apparent Fig. 4. It is well known that due to its sesquilinearity, the continuous Wigner function (5) of a signal localized at two distinct regions of phase space (known as Schrödinger-cat states) shows their interference as a third highly oscillating region between the two component terms (the *smile* of the cat). In the case of the discrete Wigner function on the torus [Eq. (8)] in Fig. 4, the I-shaped feature of the "living" Wigner function centered on $(0,0)$ is accompanied by three (approximately) similar *phantom* features, displaced in position and in momentum by $m,k \approx \pm \frac{1}{2}N$ (that appear cut by the equivalent boundary lines). These phantoms can be understood as Schrödinger cat smiles between the signal and itself, repeated modulo N around the two circles of the torus, and centered on the antipodes, $(0, \pm \frac{1}{2}N)$, $(\pm \frac{1}{2}N, 0)$, and $(\pm \frac{1}{2}N, \pm \frac{1}{2}N)$. In particular, the phantom strip in Fig. 4 casts no shadow: Its position marginal (i.e., the sum of the Wigner function over momentum k in this strip) is zero. Finally, it is important to realize that under the Fresnel shear of Fig. 1, a classical toroidal manifold must *break* somewhere. To conserve parity (11), this occurs at the two momentum circles $k \approx \pm \frac{1}{2}N$, as shown in Fig. 3.

4. EXPONENTIAL OF THE SECOND-DIFFERENCE MATRIX

Generally, a finite periodic homogeneous and isotropic system of N elements can be modeled by an $N \times N$ Hamiltonian matrix that is circulating and symmetric, $\mathbf{H} = \|H_{m,m'}\| = \mathrm{circ}(H_{|m-m'|})$, containing N dynamic parameters. The time evolution of its states, $\mathbf{f}(z) = \|f_m(z)\|$, $f_m(z) \equiv f_{m+N}(z)$, is given by the one-parameter group of matrices $\mathbf{F}(z)$ defined by

$$\mathbf{H}\mathbf{f}(z) = -\mathrm{i}\frac{\mathrm{d}}{\mathrm{d}z}\mathbf{f}(z) \Rightarrow \mathbf{f}(z) = \mathbf{F}(z)\mathbf{f}(0), \quad \mathbf{F}(z) := \exp(\mathrm{i}z\mathbf{H}). \tag{13}$$

The $z \to 0$ limit of the group line is $\mathbf{F}(z) \approx \mathbf{1} + \mathrm{i}z\mathbf{H}$, so their tangents will differ as much as their generator matrices do, times z. Different choices of the Hamiltonian matrix $\mathbf{H}$ will give rise to generally distinct z-evolution paths for the signals $\{f_m(z)\}$. We may expect that various likely

choices for free Hamiltonians will lead to quite different signal shapes; for this reason we draw attention to their signature in phase space. A natural finite analog to the purely kinetic free Hamiltonian $\frac{1}{2}\mathcal{P}^2$ is the second-difference $N\times N$ matrix $-\frac{1}{2}\mathbf{\Delta}$. This system can be visualized as a circular lattice of equal masses joined to their first neighbors by equal springs; it realizes a first, mechanical version of the finite Fresnel transform that we indicate as $\mathbf{F}^{[1]}(z)$.

The finite Fourier transform [with the discrete Fourier transform (DFT) matrix $\mathbf{\Phi}=\|\Phi_{k,m}\|$] of the second-difference matrix is diagonal:

$$\mathbf{\Delta} := \mathrm{circ}(-2,1,0,\ldots,0,1), \tag{14}$$

$$\tilde{\mathbf{\Delta}} := \mathbf{\Phi}\mathbf{\Delta}\mathbf{\Phi}^{-1} = \mathrm{diag}(-4\sin^2(\pi k/N)), \tag{15}$$

$$\Phi_{k,m} := \frac{1}{\sqrt{N}}\exp\left(-\frac{2\pi\mathrm{i}}{N}km\right), \tag{16}$$

for k, m counted modulo N in a symmetric interval. We identify the indices m and k as position and momentum, respectively. The first version of the finite Fresnel transform is the summation kernel given by the matrix

$$\mathbf{F}^{[1]}(z) := \exp\left(-\mathrm{i}\tfrac{1}{2}z\mathbf{\Delta}\right) = \mathbf{\Phi}^{-1}\exp\left(-\mathrm{i}\tfrac{1}{2}z\tilde{\mathbf{\Delta}}\right)\mathbf{\Phi} = \|F^{[1]}_{m,m'}(z)\|, \tag{17}$$

$$F^{[1]}_{m,m'}(z) = \frac{1}{N}\sum_k \exp\left(2\mathrm{i}z\sin^2\frac{\pi}{N}k\right)\exp\left(\frac{2\pi\mathrm{i}}{N}k(m-m')\right), \tag{18}$$

where we abbreviate the sum as indicated above.

The matrix (17) is unitary, $F^{[1]}_{m,m'}(-z)=F^{[1]}_{m',m}(z)^*$, and thus preserves the common sesquilinear inner product, indictated as $\langle\mathbf{f}|\mathbf{g}\rangle := \Sigma_m f^*_m g_m$. As in the continuous case these matrices form a group for $z\in\mathsf{R}$; it is not periodic when the distinct values of $\sin^2\pi k/N$ are incommensurable. In Fig. 5 we show the evolution of the centered rectangle signal of Fig. 4 under the first Fresnel matrix $F^{[1]}_{m,m'}(z)$ in Eq. (18) for various values of z and its corresponding discrete Wigner function (8) on the torus.

5. FOURIER-TRANSFORMED FRESNEL LENS

In paraxial optics, a Fresnel lens of power z multiplies the wave field by $\exp(\mathrm{i}\frac{1}{2}zx^2)$; placing this between a direct and an inverse Fourier transformer yields free propagation according to the matrix identity

$$\begin{pmatrix}0 & -1\\ 1 & 0\end{pmatrix}\begin{pmatrix}1 & 0\\ -z & 1\end{pmatrix}\begin{pmatrix}0 & 1\\ -1 & 0\end{pmatrix} = \begin{pmatrix}1 & z\\ 0 & 1\end{pmatrix}. \tag{19}$$

We can build a finite analog to this construction by replacing the Fourier integral transform by the DFT matrix $\mathbf{\Phi}$ in Eq. (16) and representing the Fresnel lens by the diagonal matrix obtained through Eq. (7),

$$\mathbf{L}(z) = \mathrm{diag}(\exp[2\mathrm{i}z(\pi m/N)^2]), \tag{20}$$

in the symmetric interval $m\in\{-\frac{1}{2}(N-1),\ldots,0,\ldots,\frac{1}{2}(N-1)\}$. This defines a *second* discrete version of the Fresnel transform by

$$\mathbf{F}^{[2]}(z) := \mathbf{\Phi}^{-1}\mathbf{L}(z)\mathbf{\Phi} = \|F^{[2]}_{m,m'}(z)\|, \tag{21}$$

$$F^{[2]}_{m,m'}(z) = \frac{1}{N}\sum_k \exp\left[2\mathrm{i}z\left(\frac{\pi k}{N}\right)^2\right]\exp\left(\frac{2\pi\mathrm{i}}{N}k(m-m')\right), \tag{22}$$

and again we have a one-parameter group of unitary matrices. The rows and columns of these matrices are not pe-

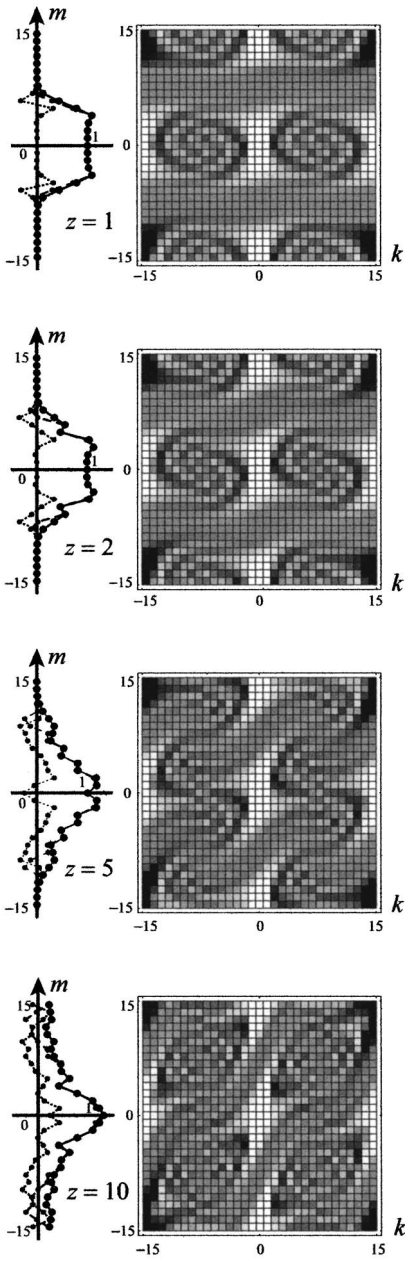

Fig. 5. Left, evolution of the centered discrete rectangle signal $\mathrm{Rect}_{-5,5}(m)$ for $N=31$ points under the first Fresnel transform $\mathbf{F}^{[1]}(z)$ for $z=1,2,5,10$. For visibility, the real, imaginary, and absolute values of the discrete points are joined by dashed, dotted, and continuous curves, respectively. Right, their corresponding Wigner functions on the 31×31 discrete torus.

riodic, so the symmetry of the range of m in Eq. (20) is important.

The evolution of the rectangle signal under this second finite Fresnel transform is shown in Fig. 6, together with the corresponding Wigner functions. We note that this transform is periodic in z modulo $z_N := N^2\pi$, since $\mathbf{F}^{[2]}(z_N)=\mathbf{1}$, as if each of the fixed-k momentum circles of the discrete phase space torus rotated through an integer number of turns. In Fig. 6 we see that at $z_1 := z_N/N$ (for $z_1 = 31/\pi \approx 10$) the centered I-shaped feature of the Wigner function *reconnects* with its copy at $(\approx \pm\frac{1}{2}N, 0)$; at one half this distance, $z_{1/2} := N/2\pi$ ($z_{1/2} \approx 5$ in the figure),

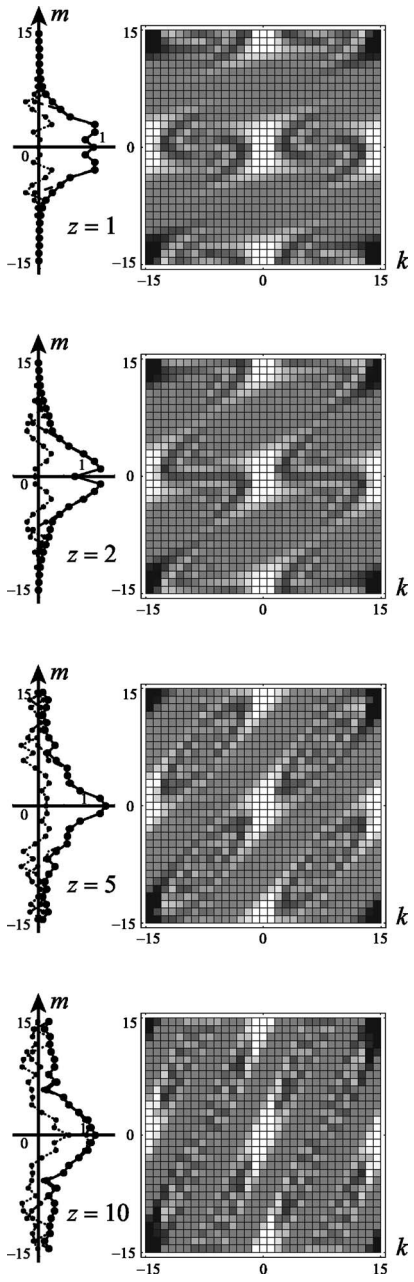

Fig. 6. Left, evolution of the rectangle signal $\mathrm{Rect}_{-5,5}(m)$ under the second Fresnel transform $F^{[2]}_{m,m'}(z)$, with the same values of $z=1,2,5,10$ and indications of real, imaginary, and absolute values. Right, their corresponding Wigner functions on the phase space torus. We note that at $z \approx 5$ and $z \approx 10$, the Wigner function band reconnects with its copies.

the Wigner function reconnects with its antipode $(\approx \pm\frac{1}{2}N, \approx \pm\frac{1}{2}N)$. Retrospectively, we recognize the same approximate features in Fig. 5, although they are less distinct due to the nonlinear values of $\sin^2 \pi k/N$ in the exponent of Eq. (18).

6. DISCRETE GAUSSIAN KERNEL

From applications to data handling of finite pixellated images that simulates near-field diffraction, Ojeda-Castañeda and colleagues [6–8] noted that the continuous Fresnel transform in Eq. (2) could be assembled—for $z=1$ only—according to the matrix product

$$\begin{bmatrix} 1 & 1 \\ 0 & 1 \end{bmatrix} = \begin{bmatrix} 1 & 0 \\ 1 & 1 \end{bmatrix} \begin{bmatrix} 0 & 1 \\ -1 & 0 \end{bmatrix} \begin{bmatrix} 1 & 0 \\ 1 & 1 \end{bmatrix}, \tag{23}$$

which corresponds to two Fresnel lenses of unit power, each of which impresses a phase $\exp(\mathrm{i}\frac{1}{2}x^2)$, on both sides of a Fourier transformer. In the continuous case, the integral kernel (4) is the phase $\exp[\mathrm{i}\frac{1}{2}(x-x')^2]$. Distinct from the spacing in Eq. (7), the correspondence here is with the centered array $x_m = \sqrt{2\pi/N}m$.

This defines a *third* finite analog for the Fresnel integral kernel that is given by the matrix $\mathbf{F}^{[3]} = \|F^{[3]}_{m,m'}\|$, with elements

$$F^{[3]}_{m,m'} := \frac{1}{\sqrt{N}} \exp\left(-\frac{\mathrm{i}\pi}{N}(m-m')^2\right). \tag{24}$$

The same discretization of the continuous Fresnel transform kernel (4) has been also used by Leonhardt as a model for precession tomography [9]. The Fresnel matrix $\mathbf{F}^{[3]}$ is the Fourier transform of Eq. (22) for $z_{1/2}=N/2\pi$; it is circulating and periodic in rows and columns.

The authors of [8] define $\mathbf{F}^{[3]}(z) := (\mathbf{F}^{[3]})^z$ for multiples of $z_{1/2}$, even though these powers do *not* have the same discrete Gaussian form with an exponent linear in z. In Fig. 7 we show the transformations of the same rectangle signal of Figs. 5 and 6 under this third Fresnel matrix $(\mathbf{F}^{[3]})^z$ in Eq. (24), and their corresponding Wigner functions (8) on toroidal phase space. Here applies again the argument on the reconnection of the sheared bands of the Wigner functions seen in Figs. 5 and 6.

The contraction $N \to \infty$ of the three models of the Fresnel transform to the continuous one follows the same limit as the DFT to the Fourier integral transform, with Kronecker δs becoming Dirac δs and the second difference matrix a second derivative (for example, see [4], Section 3.4). Thus, all three models satisfy the requirement of being finite versions of a free system. When N is large (but as all numerical data, finite) and the support of the signal is far from that of its phantoms, reasonable finite approximations $\mathbf{F}(z)$ to the Fresnel integral transform $\mathcal{F}(z)$ are achieved for small values of z. The previous finite transforms are moreover fast, since the fast Fourier transform (FFT) algorithm can be enlisted for their numerical computation. Nevertheless, we believe that the topological obstruction due to the hole in the torus seriously questions the adequacy of this phase space model of discrete systems to globally support the Fresnel transformation. In the next section we shall present a distinct fi-

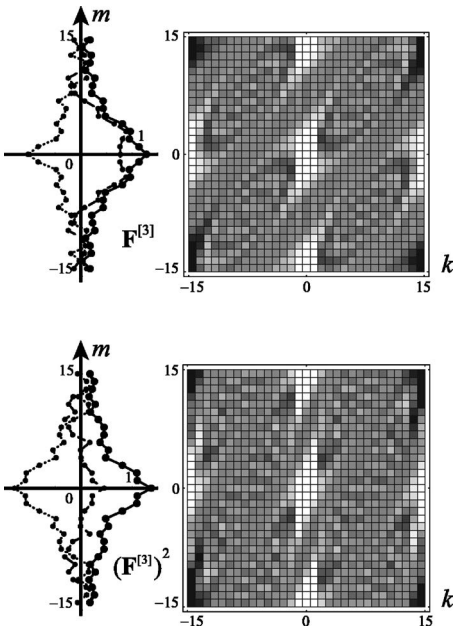

Fig. 7. Left, rectangle function $\mathrm{Rect}_{-5,5}(m)$ of Figs. 5 and 6 under the third Fresnel transform $(F^{[3]})^z$ for integer powers $z=1,2$. Right, the corresponding Wigner functions on the phase space torus.

nite analogue of the Fresnel transform on a model of finite systems whose phase space is not a torus, but a sphere. There, the breakup of phase space and the fourfold quasi-redundancy of the Wigner function on the torus are eliminated.

7. FRESNEL–KRAVCHUK TRANSFORMS

In [10] (see also [11]) we proposed a model for dynamic systems where the set of values of the position and momentum coordinates, $\{x\}$, $\{p\}$, are the spectra of two noncommuting operators $\mathcal{X}$ and $\mathcal{P}$ within a Lie algebra. When this algebra is the Heisenberg–Weyl algebra, their commutator is $[\mathcal{X},\mathcal{P}]=\mathrm{i}1$, and one has the basic construct of Schrödinger mechanics and of Fourier optics. But when one postulates that their commutator be related to the Hamiltonian of a system, several possibilities arise. In particular, the well-known angular momentum (spin) algebra su(2) (which generates the group of 2×2 unitary matrices [22]) leads to the model of a finite harmonic oscillator, where the spectra of positions, momenta, and energies are intrinsically finite and equal in spacing and number.

Consider the three traditional generators of quantum angular momentum, $\mathcal{L}_1,\mathcal{L}_2,\mathcal{L}_3$, and the new assignments for position and momentum, distinguished with overbars:

$$\text{position: } \bar{\mathcal{X}} \leftrightarrow \mathcal{L}_1, \tag{25}$$

$$\text{momentum: } \bar{\mathcal{P}} \leftrightarrow \mathcal{L}_2. \tag{26}$$

Their commutator is the third generator ℓ_3, satisfying

$$[\mathcal{L}_3,\bar{\mathcal{X}}]=\mathrm{i}\bar{\mathcal{P}}, \quad [\bar{\mathcal{P}},\mathcal{L}_3]=\mathrm{i}\bar{\mathcal{X}}, \quad [\bar{\mathcal{X}},\bar{\mathcal{P}}]=\mathrm{i}\mathcal{L}_3. \tag{27}$$

For integer or half-integer spin ℓ, these operators have matrix representations of dimension $N=2\ell+1$, where the spectra of $\bar{\mathcal{X}}$, $\bar{\mathcal{P}}$, and $\mathcal{L}_3$ are $m,k,\mu\in\{-\ell,-\ell+1,\ldots,\ell\}$, respectively. Complementing Eqs. (25) and (26), the Hamiltonian $\mathcal{H}$ is assigned to the generator of rotations around the 3-axis through

$$\mathcal{H} \coloneqq \bar{\mathcal{N}}+\tfrac{1}{2}1 \coloneqq \mathcal{L}_3+\left(\ell+\tfrac{1}{2}\right)1, \tag{28}$$

where $\bar{\mathcal{N}}$ is the *number* operator, whose eigenvalues $n \coloneqq \mu+\ell$ are the integers in $[0,2\ell]$. The three commutators in Eq. (27) are, respectively, the geometric, dynamic, and algebraic postulates of the su(2) finite oscillator model.

In this scheme, a finite N-point signal $\mathbf{f}=\{f_m\}_{m=-\ell}^{\ell}$ is a state vector in the eigenbasis of positions; using the economic bracket notation of Dirac, this is

$$f_m = {}_1\langle \ell,m|\mathbf{f}\rangle, \quad m\big|_{-\ell}^{\ell}. \tag{29}$$

Correspondingly, the momentum and (displaced) energy content of the signal $\mathbf{f}$ are its overlaps with the momentum and energy eigenbases, ${}_2\langle \ell,k|\mathbf{f}\rangle$ and ${}_3\langle \ell,\mu|\mathbf{f}\rangle$, respectively. Thus, the momentum representation of the signal is found rotating the 1-axis onto the 2-axis by means of a $\frac{1}{2}\pi$ turn around the 3-axis; this takes the place of the finite Fourier transform used in the previous sections and is called the Fourier–Kravchuk transform [10]. Whereas the unique definition of a fractional DFT matrix is problematic [14], the fractional Fourier–Kravchuk matrix of power α, $\mathbf{K}^{(\alpha)}=\|K^{(\alpha)}_{m,m'}\|$, represents a rotation by the angle $\frac{1}{2}\pi\alpha$ around the 3-axis in the position basis,

$$\begin{aligned} K^{(\alpha)}_{m,m'} &\coloneqq {}_1\left\langle \ell,m\left|\exp\left(-\mathrm{i}\tfrac{1}{2}\pi\alpha\bar{\mathcal{N}}\right)\right|\ell,m'\right\rangle_1 \\ &= e^{\mathrm{i}\pi(m'-m)\alpha/2} d^{\ell}_{m,m'}\left(\tfrac{1}{2}\pi\alpha\right), \end{aligned} \tag{30}$$

where $d^{\ell}_{m,m'}(\theta)=d^{\ell}_{m',m}(-\theta)$ are the Wigner little-d functions [[22], Eq. (3.65)],

$$\begin{aligned} d^{\ell}_{m,m'}(\theta) &\coloneqq {}_3\langle \ell,m|e^{-i\theta\mathcal{L}_2}|\ell,m'\rangle_3 \\ &= \sqrt{(j+m)!\,(j-m)!\,(j+m')!\,(j-m')!} \\ &\quad\times \sum_n \frac{(-1)^n\left(\cos\frac{1}{2}\theta\right)^{2\ell-2n+m-m'}\left(\sin\frac{1}{2}\theta\right)^{2n-m+m'}}{n!\,(\ell+m-n)!\,(\ell-m'-n)!\,(m'-m+n)!}, \end{aligned} \tag{31}$$

which are homogeneous polynomials of degree 2ℓ in the trigonometric functions and may thus be written in terms of Kravchuk polynomials in m (see [11]). The $\mathbf{K}^{(\alpha)}$'s are a group of unitary matrices with α modulo 4, which contract to the fractional Fourier integral transform when $\ell\to\infty$ [23].

The Fresnel–Kravchuk transform matrix, $\mathbf{F}^{[\mathrm{K}]}(a)=\|F^{[\mathrm{K}]}_{m,m'}(a)\|$, is generated by $\frac{1}{2}\bar{\mathcal{P}}^2$ on the position basis,

$$F^{[\mathrm{K}]}_{m,m'}(a) := {}_1\Big\langle \ell, m \Big| \exp\Big(-\mathrm{i}a\tfrac{1}{2}\bar{\mathcal{P}}^2\Big) \Big| \ell, m' \Big\rangle_1 \tag{32}$$

$$= \sum_{k=-\ell}^{\ell} {}_1\langle \ell, m | \ell, k \rangle_{22} \Big\langle \ell, k \Big| \exp\Big(-\mathrm{i}a\tfrac{1}{2}\bar{\mathcal{P}}^2\Big) \Big| \times | \ell, k \rangle_{22} \langle \ell, k | \ell, m' \Big\rangle_1 \tag{33}$$

$$= (-\mathrm{i})^{m+m'} \sum_{k=-\ell}^{\ell} d^{\ell}_{m,k}\Big(\tfrac{1}{2}\pi\Big) \times (-1)^k \exp\Big(\mathrm{i}a\tfrac{1}{2}k^2\Big) d^{\ell}_{k,m'}\Big(-\tfrac{1}{2}\pi\Big), \tag{34}$$

$$\text{i.e.,} \quad \mathbf{F}^{[\mathrm{K}]}(a) := \mathbf{K}^{(1)} \,\mathrm{diag}\Big(\exp\Big(\mathrm{i}a\tfrac{1}{2}k^2\Big)\Big)\mathbf{K}^{(-1)}. \tag{35}$$

In obtaining Eq. (34) we have used common angular momentum identities [22] and the fact that $\bar{\mathcal{P}}^2$ is diagonal in the momentum basis. Noting the structural resemblance of this Fresnel–Kravchuk transform matrix with the first two discrete Fresnel transforms, $\mathbf{F}^{[1]}(z)$ in Eq. (17) and $\mathbf{F}^{[2]}(z)$ in Eq. (21), we see that the DFT matrix $\mathbf{\Phi}$ there is replaced here with the Fourier–Kravchuk matrix $\mathbf{K}^{(1)}$, while the diagonal Gaussian phase matrix is the same as that of a finite Fresnel lens, except for the scale of the parameter a here versus z there; the conversion factor is $a = z(\pi/N)^2$.

The Fresnel–Kravchuk transform matrices $\mathbf{F}^{[\mathrm{K}]}(a)$ in Eq. (35) are unitary, *i.e.* $\mathbf{F}^{[\mathrm{K}]}(-a) = (\mathbf{F}^{[\mathrm{K}]}(a))^{\dagger}$, and form a one-parameter group in the parameter a, which is periodic modulo 4π. The spin group implies further—broken—symmetries: for $a = n\pi$ (n integer), the transform multiplies the signal values f_m by i^n for m even, while respecting those of m odd. In particular, for $n = \pm 2$ modulo 4, alternate signal values f_m reverse signs, but in all cases the absolute values are conserved (for $N = 2\ell + 1$ points, with ℓ integer). These broken symmetries will be further commented upon in the context of the Wigner function below.

The Fresnel–Kravchuk matrix represents our fourth version of the finite Fresnel transform; it acts on column-vector signals (29) in the same way as the three previous ones and will be illustrated for a rectangle function as before. However, to describe its action on the larger scenario of phase space, we must first review this basic concept in the context of the su(2) model for finite systems.

8. WIGNER FUNCTION ON THE SPHERE

In order to be consistent with the su(2) model for finite systems, where N-point signals can be specified by their position, momentum, or energy values, we are led to consider a *three*-dimensional *meta*-phase space $\vec{v} = (v_1, v_2, v_3) \in \mathsf{R}^3$, where $(v_1, v_2) = (x, p)$ will be the analog coordinates of classical phase space. This construction was introduced in [12] and generalized in [13] for any finite-dimensional Lie algebra. We proceed to offer a succinct review of the theory before displaying the action of the Fresnel–Kravchuk transform on a discrete rectangle function in a form that is readily comparable with the previous three versions of the Fresnel transform.

First, one defines a Wigner operator as an integral over the three-dimensional group manifold $g(\vec{w}) \in \mathsf{SU}(2) = \mathsf{S}^3$ (the three-sphere [12]),

$$\mathcal{W}(\vec{v}) := \int_{\mathsf{su}(2)} \mathrm{d}g(\vec{w}) \exp \mathrm{i}[w_1(v_1 - \mathcal{L}_1) + w_2(v_2 - \mathcal{L}_2) + w_3(v_3 - \mathcal{L}_3)], \tag{36}$$

where $\vec{v} \in \mathsf{R}^3$ and where $\mathrm{d}g(\vec{w})$ is the invariant Haar measure over the group ([24], Section 3.V). This is a generalization of the standard Wigner operator on the Heisenberg-Weyl group that can be symbolically written as $\sim \delta(x - \mathcal{X})\delta(p - \mathcal{P})$ [25]. The operators (36) are elements of the SU(2) group *ring* [26] and may be seen as the Fourier transform of the group itself. It is convenient to parametrize the rotation group in *polar* coordinates, i.e., as a rotation by ψ around the unit axis $\hat{u}(\theta, \phi)$ on the two-sphere S^2,

$$\vec{w} = \psi\hat{u}(\theta,\phi) = \begin{pmatrix} w_1 \\ w_2 \\ w_3 \end{pmatrix} = \begin{bmatrix} \psi \sin\theta \sin\phi \\ \psi \sin\theta \cos\phi \\ \psi \cos\theta \end{bmatrix}, \quad \begin{cases} 0 \le \psi < 2\pi \\ 0 \le \theta \le \pi \\ 0 \le \phi < 2\pi \end{cases}. \tag{37}$$

(We gloss over the important topological difference between the spin SU(2) and the rotation groups—we actually work with the latter for ℓ integer and N odd.) Similarly, $\vec{v} \in \mathsf{R}^3$ will be expressed in the spherical coordinates (v, β, γ) of radius, colatitude, and azimuth with respect to the 1-axis of positions, as in Fig. 8.

Then the su(2) Wigner *function* of an N-point signal $\mathbf{f} = \|f_m\|$, with discrete, finite position $m \in \{-\ell, -\ell$

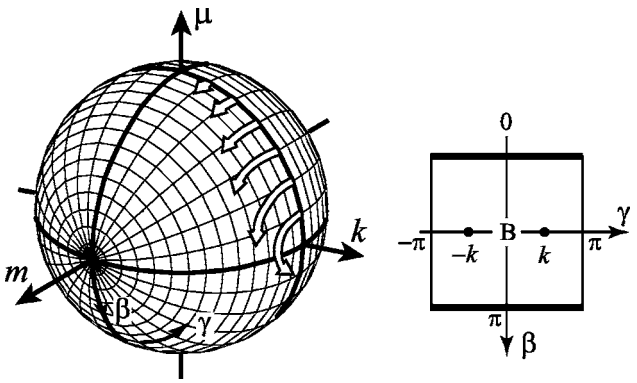

Fig. 8. Left, geometric picture of the action of the Fresnel–Kravchuk transform $\mathbf{F}^{[\mathrm{K}]}(a)$ on the sphere, which is embedded in the meta-phase space $(m, k, \mu) \in \mathsf{R}^3$ of position, momentum, and (displaced) energy; the polar angles (β, γ) are determined by the position and energy axes. The transform wrings the sphere around the momentum k axis, rotating it differentially by angles $\sim \frac{1}{2}ak^2$, as shown by the empty arrows. Right: We represent the surface of the sphere by its coordinates (β, γ) drawn on a plane to present the su(2) Wigner function in a form directly comparable with the three previous versions of the discrete Fresnel transform on the torus. The center (B) corresponds to the "bottom pole" of ground energy at $(\beta = \frac{1}{2}\pi, \gamma = 0)$. The $\pm k$ points $(\beta = \frac{1}{2}\pi, \gamma = \pm\frac{1}{2}\pi)$ are the two extreme "momentum poles." The left and right lines at $\gamma = \pm\pi$ are the "top meridian" of the sphere. The top and bottom heavy lines correspond to the singular points $\beta = 0$ and π of the polar coordinate system at the upper and lower extremes of the position m axis.

$+1,\ldots,\ell\}$, $N=2\ell+1$, is the expectation value of the Wigner operator (36) in that state,

$$W^{(\ell)}(\mathbf{f}|\vec{v}) := \langle \mathbf{f}|\mathcal{W}(\vec{v})|\mathbf{f}\rangle = \sum_{m,m'=-\ell}^{\ell} f_m^* W^{(\ell)}_{m,m'}(\vec{v}) f_{m'}, \qquad (38)$$

where the last expression introduces what we may call the Wigner *matrix* $\mathbf{W}^{(\ell)}(\vec{v}) = \| W^{(\ell)}_{m,m'}(\vec{v}) \|$, which is self-adjoint. The covariance of Eq. (36) with rotations allows one to express this matrix in terms of its diagonal form

$$W^{(\ell)}_{m,m'}(v,\beta,\gamma) = e^{-\mathrm{i}(m-m')\gamma} \sum_{\bar{m}=-\ell}^{\ell} d^{\ell}_{m,\bar{m}}(\beta) \bar{W}^{(\ell)}_{\bar{m}}(v) d^{\ell}_{\bar{m},m'}(-\beta). \qquad (39)$$

Finally, the diagonal form, which is a function only of the radius v, is found to be [12]

$$\bar{W}^{(\ell)}_{\bar{m}}(v) = (-1)^{2\ell+1} \frac{\pi}{2} \sum_{m=-\ell}^{\ell} \int_0^{\pi} \sin\beta \mathrm{d}\beta \times |d^{\ell}_{\bar{m},m}(\beta)|^2 \frac{\sin(2\pi v \cos\beta)}{(v\cos\beta - m)[(v\cos\beta - m)^2 - 1]}, \qquad (40)$$

where we note that in the integrand, the numerator, and the denominator have canceling zeros at $v\cos\beta = m, m\pm 1$.

The diagonalized matrix $\bar{\mathbf{W}}^{(\ell)}(v)$ still depends on the radius $v>0$; but since the SU(2)-invariant Casimir operator $\vec{\mathcal{L}}^2 := \Sigma_{n=1}^3 \mathcal{L}_n^2$ is $\ell(\ell+1)1$, one expects the Wigner function of any $N=2\ell+1$-point signal to be concentrated to a spherical shell of squared radius $v^2 \approx \ell(\ell+1)$. And indeed, calculation of the trace of Eq. (40) shows that it is strongly peaked in the range $\ell < v < \ell+1$, with very small values oscillating around zero elsewhere ([12], Fig. 2). Computation of the Wigner function (38) for various values of $|\vec{v}|$ show suprisingly similar plots differing only in scale. In fact, in [27] it was shown that the radial integration of the su(2) Wigner function (36) returns the Stratonovich–Agarwal Wigner function for spin systems over the sphere [28,29]. Thus we compute and display our results for the radius $v=\ell+\frac{1}{2}$ and reduce our consideration of metaphase space to the phase space sphere S^2, with coordinates (β,γ), where the point $\beta=0$ is in the positive direction of the 1-axis of positions, as shown in Fig. 8.

The action of the Fresnel–Kravchuk transform on the phase space sphere can now be understood in the following way: Whereas the fractional Fourier–Kravchuk transform generated by $\mathcal{L}_3$ rotates the sphere of Fig. 8 around the 3-axis, and generally $\exp(\mathrm{i}\psi\hat{u}\cdot\vec{\mathcal{L}})$ will rigidly rotate the sphere by ψ around the axis $\hat{u}(\theta,\phi)$, the Fresnel–Kravchuk transform $\exp\left(-\mathrm{i}\alpha\frac{1}{2}\vec{\mathcal{P}}^2\right)$ is a nonrigid ("differential") rotation that wrings the sphere around the 2-axis of momenta as if each $p=$constant circle were rotated by a different angle $\frac{1}{2}ap$. The "as if" refers to the fact that under nonlinear transformations—aberrations—of phase space, the Wigner function is not simply carried along with its underlying manifold but develops wiggles and revivals, as was shown in [30,31] for continuous and finite systems, respectively.

Thus, given an N-point signal vector $\mathbf{f}$, its Fresnel–Kravchuk transform will be the vector $\mathbf{f}(a)=\mathbf{F}^{[\mathrm{K}]}(a)\mathbf{f}$, obtained through straightforward multiplication by the Fresnel–Kravchuk matrix (32), and its su(2) Wigner function will be thereafter obtained from Eq. (38). In Fig. 9 we display the results for the rectangle signal of the previous sections, using the evolution parameter $z=a(N/\pi)^2$ to ease the comparison. The su(2) Wigner function of the rectangle (for $z=0$) has a well-defined peak ($W=5.8164$ at

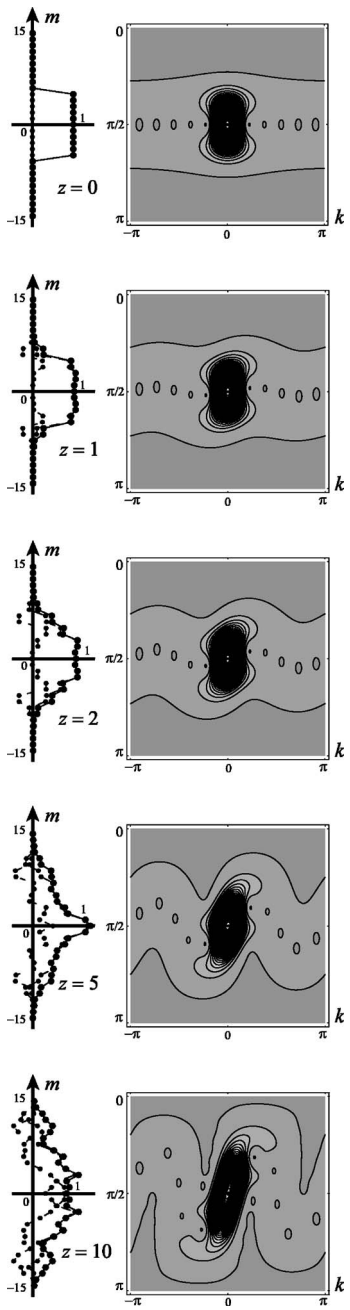

Fig. 9. Left, evolution of the rectangle function $\mathrm{Rect}_{-5,5}(m)$ under the Fresnel–Kravchuk transform $\mathbf{F}^{[\mathrm{K}]}(a)$ for $N=31$ ($\ell=15$), $a=z(\pi/N)^2\approx 0.010270z$, and $z=0,1,2,5,10$. Right, the corresponding Wigner functions on the su(2) phase space sphere (β,γ); it is displayed on the (β,γ) plane as explained in Fig. 8.

$\beta=\frac{1}{2}\pi$, $\gamma=0$) that resembles the peak of the continuous case in Fig. 2; however, it oscillates far less. We used 40 contours to emphasize the structure of the regions where it has small negative values that occur on the line $\beta=\frac{1}{2}\pi$. Yet it is surprising how small they are: For $\gamma=\pm 0.7099$, ± 1.1959,± 1.7431, ± 2.3003, and ± 2.8609 (radians), the Wigner function there has values $W=-1.1306\times 10^{-8}$, -2.6719×10^{-8}, -4.5053×10^{-8}, -8.2010×10^{-8}, and -5.9180×10^{-6}, respectively. We noted that for rectangle functions $\mathrm{Rect}_{-n,n}(m)$ there are n of these negative dimples. Outside the main peak the Wigner function is very small: For $(\beta,\gamma)=(\frac{1}{2}\pi,\pm\pi)$ it is 0.0114.

Regarding the symmetries of the Wigner function under Fresnel–Kravchuk evolution of the signal, we recall [31] that the su(2) model also provided the description of the Kerr anomaly generated by the square of the harmonic oscillator Hamiltonian (here $\mathcal{L}_3$), which is only a rotation of the Fresnel transform around the position axis by $\frac{1}{2}\pi$. The symmetry properties of the Wigner function that follow from the parity and complex conjugation symmetries of the signal are closely analogous to Eqs. (11) and (12). Here they read

$$f_{-m}=\pm f_m \Rightarrow W^{(\ell)}(f|v,\beta,\gamma)=W^{(\ell)}(f|v,\pi-\beta,-\gamma), \quad (41)$$

$$f^{*}_{m}=\pm f_m \Rightarrow W^{(\ell)}(f|v,\beta,\gamma)=W^{(\ell)}(f|v,\beta,-\gamma). \quad (42)$$

There are no phantoms on the sphere, and the whole Wigner function is living. The symmetries of the Fresnel–Kravchuk transform at $\alpha=n\pi$ (n modulo 4) that we commented on above can be readily recognized. For $\alpha=\pm 2\pi$, low- and high-energy values are exchanged: The peaks in Figs. 9 that are at the bottom pole of Fig. 8, after wiggling wildly, re-form at the top pole, as if the sphere rotated by $\pi=\frac{1}{2}\alpha$ around the position axis [the factor $\frac{1}{2}$ is in Eqs. (32)–(35)]. For $\alpha=\pm\pi$ the Wigner function consists of two approximate copies of the peak at both the top and bottom poles, with a small interference smile between them. This corresponds to the n-eyed Schrödinger cat states shown in ([12], Fig. 5) for coherent states under Kerr evolution at fractions π/n; since our test function is a sharp-edged rectangle, this is clearly visible only for $n=2$. The periodicity reminds us of the Talbot effect.

9. CONCLUSIONS

We chose the rectangle step signal to compare the integral and the finite Fresnel transforms because it highlights the oscillatory behavior of the resulting functions in Fig. 2 versus those in Figs. 5–7 and 9.

The figures suggest four evolution phases: First (up to $z=1$), the integral transform oscillates rapidly with a Gibbslike chirp overshoot of $\approx 17.5\%$ near to the rectangle edge; the finite versions approximate this by rough plateaus. Second (around $z=2$), the oscillations of smaller wavelengths dampen, the main body of the function thins, and its overshoots grow to $\approx 25\%$, shaping two peaks; this phase is also apparent in the finite versions but varies considerably from one version to another. Third (around $z=5$), the two peaks coalesce with an overshoot of $\approx 33\%$; the finite versions do so, too, roughly. And fourth ($z=10$ and beyond), the peak slowly decreases and diffuses over the full real line; finite versions cannot diffuse indefinitely, so the four distinct transforms we examined keep oscillating, each following its own dynamics with occasional revivals, but all resemblance to the continuous case is lost. As all aberrations, the finite Fresnel transforms follow the continuous model only for small values of the evolution parameter. Beyond some point dependent on the dynamics of the model, the finite approximation will no longer be faithful to its continuous prototype.

To evaluate the fidelity of the four versions of the finite Fresnel transform to approximate the Fresnel integral transform, we can choose to compare their action on phase space, rather than on signals; particularly the shearing of their Wigner functions shown in the figures. Both on the torus and on the sphere one can see these shears, but the topological obstruction of the torus is evident in the rather chaotic oscillations at the breaking lines of momentum. In contrast, the geometric deformation of the sphere, although it makes the su(2) Wigner function wiggle slightly, is a smooth process under which the main peak conserves its integrity.

The su(2) finite oscillator model [10] was conceived to describe the fractional Fourierlike transform undergone by N coherent light signals in a shallow planar multimodal waveguide supporting N transverse modes. It allows for discrete coherent states that move according to the Hamilton equations of their continuous counterparts [14]. The fractional Fourier–Kravchuk transform rigidly rotates the sphere of Fig. 8 around its vertical axis; its action on the Wigner functions depicted on the (β,γ) plane of Fig. 9 will rotate it almost rigidly about the center $(\frac{1}{2}\pi,0)$, with increasing distorsion toward the edges.

There are also other valid criteria for prefering periodic or nonperiodic finite models, such as considerations on speed and simplicity versus consistency with the geometry and dynamics of mechanical and optical systems. To compute the Fresnel–Kravchuk transform (34), we cannot use the FFT algorithm, so its use for real-time analysis of most actual signals is compromised. Yet, we regard the present analysis of this finite transform as a second step toward understanding the structure of the group $\mathrm{U}(N)\supset\mathrm{SU}(2)$ of all unitary transformations of N-point signals, regarding them as aberrations of the compact phase space of finite systems.

ACKNOWLEDGMENTS

We are indebted to N. M. Atakishiyev (Instituto de Matemáticas, UNAM-Cuernavaca), G. S. Pogosyan (Departamento de Matemáticas, Universidad de Guadalajara), and L. E. Vicent (Facultad de Ciencias, Universidad Autónoma del Estado de Morelos) for discussions on the subjects of this paper. Support from the SEP–CONACYT project 44845 and DGAPA–UNAM project IN102603, Óptica Matemática, is gratefully acknowledged.

REFERENCES

1. J. W. Goodman, *Introduction to Fourier Optics* (McGraw-Hill, 1996).
2. S. A. Collins, Jr., "Lens-system diffraction integral written in terms of matrix optics," J. Opt. Soc. Am. **60**, 1168–1177 (1970).

3. M. Moshinsky and C. Quesne, "Oscillator systems," in *Proceedings of the 15th Solvay Conference in Physics (1970)* (Gordon & Breach, 1974).
4. K. B. Wolf, *Integral Transforms in Science and Engineering* (Plenum, 1979).
5. G. García-Calderón and M. Moshinsky, "Wigner distribution function and the representation of canonical transformations in quantum mechanics," J. Phys. A **13**, L185–L188 (1980).
6. V. Arrizón and J. Ojeda-Castañeda, "Fresnel diffraction of substructured gratings: matrix description," Opt. Lett. **20**, 118–120 (1995).
7. V. Arrizón, J. G. Ibarra, and J. Ojeda-Castañeda, "Matrix formulation of the Fresnel transform of complex transmittance gratings," J. Opt. Soc. Am. A **13**, 2414–2422 (1996).
8. S. C. Bradburn, J. Ojeda-Castañeda, and W. T. Cathey, "Matrix description of near-field diffraction and the fractional Fourier transform," J. Opt. Soc. Am. A **16**, 316–322 (1999).
9. U. Leonhardt, "Discrete Wigner function and quantum-state tomography," Phys. Rev. A **53**, 2998–3013 (1996).
10. N. M. Atakishiyev and K. B. Wolf, "Fractional Fourier–Kravchuk transform," J. Opt. Soc. Am. A **14**, 1467–1477 (1997).
11. N. M. Atakishiyev, G. S. Pogosyan, and K. B. Wolf, "Finite models of the oscillator," Phys. Part. Nucl. **36**, Suppl. 3 521–555 (2005).
12. N. M. Atakishiyev, S. M. Chumakov, and K. B. Wolf, "Wigner distribution function for finite systems," J. Math. Phys. **39**, 6247–6261 (1998).
13. S. T. Ali, N. M. Atakishiyev, S. M. Chumakov, and K. B. Wolf, "The Wigner function for general Lie groups and the wavelet transform," Ann. Henri Poincare **1**, 685–714 (2000).
14. K. B. Wolf and G. Krötzsch, "Geometry and dynamics in the fractional discrete Fourier transform," J. Opt. Soc. Am. A **24**, 651–658 (2007).
15. K. B. Wolf, *Geometric Optics on Phase Space* (Springer-Verlag, 2004).
16. E. P. Wigner, "On the quantum correction for thermodynamic equilibrium," Phys. Rev. **40**, 749–759 (1932).
17. M. Hillery, R. F. O'Connel, M. O. Scully, and E. P. Wigner, "Distribution functions in physics: fundamentals," Phys. Rep. **259**, 121–167 (1984).
18. M. J. Bastiaans, "Wigner distribution function applied to optical signals and systems," Opt. Commun. **25**, 26–30 (1978).
19. W. K. Wooters, "A Wigner-function formulation of finite-state quantum mechanics," Ann. Phys. (N.Y.) **176**, 1–21 (1987).
20. J. C. O'Neill and W. J. Williams, "Shift covariant time–frequency distributions of discrete signals," IEEE Trans. Signal Process. **47**, 133–146 (1999).
21. S. Korkmaz, Harmonic Analysis in Finite Phase Space, M.Sc. thesis (Institute of Engineering and Science of Bilkent University, 2005).
22. L. C. Biedenharn and J. D. Louck, "Angular Momentum in Quantum Physics," in *Encyclopedia of Mathematics and Its Applications*, G.-C. Rota, ed. (Addison-Wesley, 1981).
23. N. M. Atakishiyev, G. S. Pogosyan, and K. B. Wolf, "Contraction of the finite one-dimensional oscillator," Int. J. Mod. Phys. A **18**, 317–327 (2003).
24. R. Gilmore, *Lie Groups, Lie Algebras, and Some of their Applications* (Wiley Interscience, 1978).
25. H.-W. Lee, "Theory and applications of the quantum phase-space distribution functions," Phys. Rep. **259**, 147–211 (1995).
26. K. B. Wolf, "Wigner distribution function for paraxial polychromatic optics," Opt. Commun. **132**, 343–352 (1996).
27. S. M. Chumakov, A. B. Klimov, and K. B. Wolf, "On the connection of two Wigner functions for spin systems," Phys. Rev. A **61**, 034101(3) (2000).
28. R. L. Stratonovich, "On distributions in representation space," Zh. Eksp. Teor. Fiz. **31** 1012–1020 (1956) [Sov. Phys. JETP **4**, 891–898 (1957)].
29. G. S. Agarwal, "Relation between atomic coherent-state representation, state multipoles, and generalized phase-space distributions," Phys. Rev. A **24**, 2889–2896 (1981).
30. A. L. Rivera, N. M. Atakishiyev, S. M. Chumakov, and K. B. Wolf, "Evolution under polynomial Hamiltonians in quantum and optical phase spaces," Phys. Rev. A **55**, 876–889 (1997).
31. S. M. Chumakov, A. Frank, and K. B. Wolf, "Finite Kerr medium: macroscopic quantum superposition states and Wigner functions on the sphere," Phys. Rev. A **60**, 1817–1823 (1999).